

1  
2 **Himalaya air quality impacts from the COVID-19 lockdown across the Indo-**  
3 **Gangetic Plain**

4  
5  
6 G.W.K. Moore<sup>1,2</sup> and J.L. Semple<sup>3</sup>

7 <sup>1</sup>Department of Physics, University of Toronto

8 <sup>2</sup>Department of Chemical and Physical Sciences, University of Toronto Mississauga

9 <sup>3</sup>Department of Surgery, University of Toronto

10 Corresponding author: G.W.K. Moore ([gwk.moore@utoronto.ca](mailto:gwk.moore@utoronto.ca))

11 **Key Points:**

- 12
- 13 • The COVID-19 lockdown provides an opportunity to assess the impact of air pollution from the Indo-Gangetic Plain on the Himalaya.
  - 14 • Air pollution levels in cities in the western Indo-Gangetic Plain experienced marked drops that coincided with the lockdown.
  - 15
  - 16 • Across the Indo-Gangetic Plain and Himalaya, there were reductions in air pollution in the west and increases in the east.
  - 17
  - 18

**19 Abstract**

20 Starting in January 2020, the novel coronavirus, now known as acute respiratory syndrome  
21 coronavirus (SARS-CoV-2) and the disease that it causes (COVID-19) has had significant impacts  
22 on human health, the environment and the economy globally. The rapid lockdown that occurred  
23 as well as its well documented timing in various locations allows for an unprecedented opportunity  
24 to examine the impact of air pollution from densely populated regions has on adjacent and pristine  
25 environments. Here we use in-situ and satellite observations to show that there was a step function  
26 decrease in two key indicators of air quality, nitrogen dioxide and airborne particulates, in  
27 locations within the Indo-Gangetic Plain (IGP) as a result of the Spring 2020 lockdown. Based on  
28 anomaly patterns, we find a dipole response with a statistically significant reduction in air pollution  
29 along the western IGP and Himalaya and an increase in air pollution in the eastern IGP and  
30 Himalaya. We show that spatial variability in the reductions in economic activity across northern  
31 India and the adjoining countries of Nepal, Pakistan and Bangladesh contributed to this dipole as  
32 did a persistent atmospheric circulation anomaly across the region during the lockdown.

**33 1 Introduction**

34 The densely populated IGP that includes much of northern India, eastern Pakistan and  
35 Bangladesh, is one of the most polluted regions of the world (Lau & Kim, 2010). For example,  
36 based on fine particle pollution data from 29 U.S. diplomatic posts across the world, New Delhi  
37 ranks as the most polluted city with median air quality rated as being unhealthy with the frequent  
38 occurrence of hazardous conditions (Dhammapala, 2019). Common sources of air pollution in the  
39 region include transportation, construction, industrial activity, electricity generation and biomass  
40 burning (Ghude et al., 2011; Dhammapala, 2019). There is evidence that this pollution has the  
41 potential for increasingly dramatic impacts, as the IGP continues to industrialize, on the  
42 population, environment and climate in the relatively pristine Himalaya that form the northern

43 boundary of the IGP (Dentener et al., 2006; Moore & Semple, 2009; Ghude et al., 2011; Bonasoni  
44 et al., 2012). Please refer to Figure 1 for place names in the region of interest.

45 One common characteristic that spans most research topics in the geosciences is the  
46 inability to undertake large-scale controlled experiments that help identify processes and  
47 pathways. The existence of events characterized by step changes in external forcing often allow  
48 unique opportunities that mimic the sort of experiments that are common in laboratory-based  
49 scientific disciplines. Examples include: volcanic eruptions that result in large inputs of aerosols  
50 into the stratosphere that subsequently impact the earth's radiative balance leading to a widespread  
51 cooling (Brasseur & Granier, 1992); total solar eclipses that result in a transient reduction in  
52 incoming solar radiation that can impact meteorological processes throughout the atmospheric  
53 column (Aplin et al., 2016). There is also evidence that the cessation of air travel across the United  
54 States after September 11 2001 resulted in a reduction in contrails that impacted surface  
55 temperatures (Travis et al., 2004). However, the relatively short period, 4 days, of the cessation  
56 limited the ability to definitively attribute the presence of a signal (Hong et al., 2008).

57 In a similar vein, the COVID-19 related lockdown (Chamas, 2020; Ellis-Petersen et al.,  
58 2020) that occurred across the IGP in March 2020 offers a unique opportunity to assess the impact  
59 of pollution sources across this region on the Himalaya. We will focus attention on Nitrogen  
60 Dioxide (NO<sub>2</sub>) an important component of air pollution (WHO, 2006) in and of itself as well as  
61 being a precursor species to ozone, a pollutant and oxidant that has been shown to impact lung  
62 function (Lippmann, 1989). We will also consider airborne particulate matter with diameters  
63 smaller than 2.5 $\mu$ m (pm<sub>2.5</sub>) that have also been shown to impact human health (WHO, 2006).

64 Based on anomaly patterns, we find a dipole response during the Spring 2020 lockdown  
65 with a statistically significant reduction in air pollution along the western IGP and Himalaya as

66 well as an increase in air pollution in the eastern IGP and Himalaya. We show that spatial  
67 variability in the reductions in economic activity across northern India and the adjoining countries  
68 of Nepal, Pakistan and Bangladesh contributed to this dipole as did a persistent atmospheric  
69 circulation anomaly across the region during the lockdown.

## 70 **2 Data and Methods**

71 Data on surface concentrations of NO<sub>2</sub> for the period 2017-2020 were accessed from  
72 OpenAQ Platform. Data on surface concentrations of NO<sub>2</sub> in Delhi for the period 2005-2016 were  
73 accessed from the archives of the Central Pollution Control Board. There are multiple reporting  
74 sites within Delhi and these were averaged to obtain the time series for this city. There are  
75 individual reporting sites with the other three locations discussed in the paper: Ludhiana, Singrauli  
76 and Asansol.

77 Data on surface pm<sub>2.5</sub> concentrations were obtained from United States Embassies or  
78 Consulates in Delhi India, Lahore Pakistan, Dhaka Bangladesh and Kathmandu Nepal as archived  
79 by the Environmental Protection Agency.

80 To characterize the impact of the lockdown on the spatial and temporal variability in air  
81 quality across the IGP and the Himalaya, we use daily tropospheric NO<sub>2</sub> column retrievals from  
82 the OMI instrument (Boersma et al., 2011) on NASA's Aura satellite as well as higher spatial  
83 resolution data from the TROPOMI instrument (Veefkind et al., 2012) on ESA's Sentinel 5P  
84 satellite.

85 Daily tropospheric NO<sub>2</sub> column retrievals from the OMI instrument on NASA's Aura  
86 satellite, available from 2005-2020 at a spatial resolution of  $\frac{1}{4}^\circ$  or  $\sim 25\text{km}$  (Boersma et al., 2011),  
87 as well as the TROPOMI instrument on ESA's Sentinel 5P satellite, available from 2018-2020 at  
88 a spatial resolution of  $\sim 4\text{km}$  (Veefkind et al., 2012) were used to characterize the spatial

89 distribution of pollutants. For each dataset, the cloud cleared retrievals were used. The longer  
90 length of data availability for the OMI instrument allows for the development of a climatology.  
91 This is not possible for the TROPOMI.

92 Information on the spatial distribution of particulate matter is also available from the OMI  
93 instrument through the so-called Aerosol Index (AI) that uses differential absorption of upwelling  
94 ultra-violet radiation to indicate the presence of aerosols associated with dust, smoke and volcanic  
95 ash (Torres et al., 2007). It is available at a spatial resolution of  $1^\circ$  daily from 2005-2020 (Torres  
96 et al., 2007).

97 Mass-weighted wind data from the European Centre for Medium-Range Weather  
98 Forecasts' ERA5 Reanalysis (Hersbach et al., 2020) were used to characterize the atmospheric  
99 circulation during April 2020. The data is available at a spatial resolution of  $\sim 30\text{km}$  for the period  
100 1979-2020.

### 101 **3 Results**

102 Figure 2 shows time series of the daily mean surface concentration of  $\text{NO}_2$  at selected sites  
103 across the IGP. Please refer to Figure 1 for the locations of these sites. The data in this figure  
104 shows a step function reduction in surface  $\text{NO}_2$  concentration occurred in both Delhi (Fig 2a) and  
105 Ludhiana, (Fig 2b), large urban centers in the Indian sector of the IGP, around March 23 2020  
106 that coincided with the lockdown in the region (Chamas, 2020; Ellis-Petersen et al., 2020). The  
107 reduction in surface  $\text{NO}_2$  concentrations persisted through the end of April in these cities.  
108 Climatological surface  $\text{NO}_2$  data is available for Delhi back to 2005 and shows a seasonal decline  
109 in values during the transition from winter through the spring (Mohan & Kandya, 2007) that can  
110 also be seen in Figure 2a. A 31-day moving window smoother was applied to the climatological  
111 time series to reduce high frequency signals that are the result of their short length so as to allow

112 a clearer picture of the seasonal cycle and its variability. This inter-annual variability in surface  
113 NO<sub>2</sub> concentration confirm that values recorded in Delhi during the lockdown were two standard  
114 deviations below the mean indicating highly anomalous conditions. Indeed, the monthly mean  
115 surface NO<sub>2</sub> concentrations observed in Delhi during April 2020 were the lowest observed in the  
116 16-year climatology.

117 However, the marked reduction in surface NO<sub>2</sub> concentrations observed in Delhi and  
118 Ludhiana were not uniform across the IGP. Singrauli, a city with a number of large coal-fired  
119 power plants in its vicinity (Singh et al., 2018), recorded no reduction in surface NO<sub>2</sub>  
120 concentrations suggesting that the emissions from these plants were not reduced during the  
121 lockdown (Fig 2c). Asansol, a major industrial city with significant coal mining and steel  
122 production activities (Reddy & Ruj, 2003), in West Bengal showed a reduction in surface NO<sub>2</sub>  
123 values suggesting a more modest lockdown than what occurred in Delhi and Ludhiana.

124 Time series of pm<sub>2.5</sub> concentrations from U.S. embassies and consulates throughout the  
125 IGP (Figure 3) indicates the presence of step function reductions in both Delhi as well as Lahore  
126 Pakistan, confirming that a lockdown also occurred in the Pakistani region of the IGP. Dhaka also  
127 showed a reduction however no indication of a step function change. This is most likely a  
128 reflection of the strong seasonality in air quality in the region with a winter peak associated with  
129 kiln production (Begum et al., 2011). There was also evidence of a step function response in  
130 Kathmandu although there was significant variability throughout April indicating either an  
131 incomplete shutdown of industrial activity or the long-range transport of pollution into the area  
132 (Bonasoni et al., 2012).

133 The climatological distribution of monthly mean tropospheric NO<sub>2</sub> column densities from  
134 OMI during April (Fig 4a) shows elevated levels across the IGP with lower levels over eastern

135 India, southwestern India and Tibet. There is a gradient in density across the Himalaya that  
136 approximately follows the 3000m height contour suggesting that topography plays a role in the  
137 distribution of air pollution across the region. A number of localized maxima associated with  
138 urban centers, like Delhi, Lahore and Dhaka, or regions of industrial activity, such as Singrauli  
139 and Asansol are evident. The distribution during April 2020 (Fig 4b) shows generally lower values  
140 across much of the IGP with a marked absence of local maxima in the vicinity of Delhi and Lahore.

141 More information on the spatial variability on tropospheric NO<sub>2</sub> column densities  
142 associated with the lockdown is provided by the monthly mean anomaly during April 2020 (Fig  
143 5a), i.e. the difference between the monthly mean during April 2020 and the April climatological  
144 monthly mean for the period 2005-2020. The widespread reduction across the northwestern IGP  
145 as well as adjoining foothills of the western Himalaya, i.e. to the west of Kathmandu, is evident.  
146 The region around Singrauli stands out as one in which there was a marked increase in column  
147 density during April 2020. Throughout much of the eastern IGP, including much of Bangladesh,  
148 eastern India, eastern Nepal and Bhutan, there was an increase in column density with the  
149 exception of region around Dhaka.

150 There is of course variability from year to year in air quality that is a function of variability  
151 in sources as well as meteorological conditions (Fishman et al., 2005; Pawar et al., 2017). One  
152 way to assess the magnitude of the anomalous tropospheric NO<sub>2</sub> column densities during April  
153 2020 is to compare it to the expected variability from year to year during April. This so-called  
154 normalized anomaly is constructed by dividing the April 2020 anomaly by the standard deviation  
155 of the tropospheric NO<sub>2</sub> column density during April and expressing it as a percentage (Fig 5b).  
156 Normalized anomaly values on the order of +/- 200% indicate that such an anomaly has a  
157 magnitude of 2 standard deviations and should, assuming normally distributed data, occur

158 approximately 2-3% of the time. Across much of the western IGP, including Delhi, Ludihana and  
159 Lahore, as well as the western Himalaya, the normalized anomaly was on the order of 200%  
160 confirming the extreme reduction in air pollution in this region, a result in agreement with the  
161 surface observations of surface NO<sub>2</sub> concentration (Fig 2) and surface pm2.5 (Fig 3) across the  
162 western IGP. In contrast, the normalized anomaly across much of the eastern IGP and the eastern  
163 Himalaya was positive with values between 100% and 200% indicating that air pollution values  
164 in this region were anomalously high, although with significance levels lower than that in the west  
165 of the region of interest. This result is also in agreement with regional surface NO<sub>2</sub> concentrations  
166 during the lockdown (Fig 2) that show lower concentrations in Delhi and Ludhiana as well as  
167 higher concentratons in Singrauli and Asansol. We will refer to this feature, reduction in air  
168 pollution in the western IGP and Himalaya and an increase in the corresponding eastern regions,  
169 as an air pollutuion dipole anomaly.

170 Figures 4 & 5 indicate that there is evidence of spatial gradients in tropospheric NO<sub>2</sub>  
171 column densities along the Himalaya that may be under resolved by the OMI instrument. A  
172 comparison between TROPOMI monthly means for April 2019 and 2020 (Fig 6a&b) show clear  
173 evidence of a reduction in tropospheric NO<sub>2</sub> column densities across much of the IGP, including  
174 in the vicinity of Delhi, Lahore, Asansol and Dhaka, as well as pronounced spatial gradients along  
175 the Himalaya. The difference between the two Aprils (Fig 6c) highlights the aforementioned  
176 dipolar nature of the changes that occurred with reductions across much of the western IGP and  
177 the western Himalaya and increases in the eastern areas of these regions.

178 Observations of surface particulate matter (Fig 3) also indicated the presence of step  
179 function responses across the western IGP and Nepal that were associated with the lockdown.  
180 The climatological monthly mean AI for April (Fig 7a) indicates the presence of aerosols across

181 the western IGP with lower values over Tibet. This pattern is characteristic of so-called  
182 Atmospheric Brown Clouds, polluted tropospheric layers characterized by high values of  
183 anthropogenic aerosols (Ramanathan et al., 2007; Bonasoni et al., 2012). The monthly mean AI  
184 for April 2020 (Fig 7b) shows reduced AI values across the IGP, consistent with the in-situ  
185 observations of surface pm<sub>2.5</sub> (Fig 3). The normalized anomaly for April 2020 (Fig 7c) indicates  
186 that the reduction in AI across the western IGP and the western Himalaya was between 1 and 1.5  
187 standard deviations below the mean. Unlike the case for the tropospheric NO<sub>2</sub> column density,  
188 there is no evidence of a coherent dipolar pattern with higher values of the AI in the eastern regions  
189 of the IGP and the Himalaya.

190 Atmospheric circulation patterns play a role in the long-range transport of pollutants into  
191 relatively pristine regions such as the Himalaya (Bonasoni et al., 2012). As such it is important to  
192 characterize the degree to which the atmospheric conditions contributed to the spatial distribution  
193 of the air pollution anomalies associated with the COVID-19 lockdown across the IGP. Figure 8  
194 shows the April 2020 monthly mean anomaly in mass weighted velocity field, representative of  
195 circulation in the lower troposphere, over the region of interest as represented in the ERA5  
196 reanalysis (Hersbach et al., 2020). It indicates the presence of a cyclonic (i.e. counter-clockwise)  
197 circulation anomaly over the region. A cyclonic circulation anomaly would have acted to mitigate  
198 the transport of pollutants from the IGP towards the western Himalaya and enhance this transport  
199 towards the eastern Himalaya. As such, it would have acted to support the existence of the dipolar  
200 pattern in the distribution of pollutants along the IGP and Himalaya during April 2020.

#### 201 **4 Conclusions**

202 High mountainous regions of the world, traditionally, have been considered some of the  
203 most pristine environments and the least likely setting for hazards related to air pollution. However

204 unique communities in high-altitude regions, such as those in the Himalaya, are unexpectedly  
205 exposed to pollution levels that are similar to, if not higher than, those reported in industrialized  
206 cities and other polluted environments (Saikawa et al., 2019). However little is known about the  
207 sources for this pollution and its pathways (Bonasoni et al., 2012). In addition, hypoxia and other  
208 unique characteristics of this high altitude ecosystem have compounding consequences for those  
209 who reside in and work in this region (Pandey, 1984; Korrick et al., 1998; Semple et al., 2016).

210         The COVID-19 lockdown within the heavily polluted IGP provides a unique opportunity  
211 to assess the impact of pollution from this region on the Himalaya. The lockdown produced a  
212 dipolar signature in pollution levels across the IGP with reductions in the west, that were 2 standard  
213 deviations below the climatological mean during April 2020 and a more modest increase in the  
214 east. This was most likely the result of differences in the local response to the lockdown with large  
215 cities such as Delhi and Lahore experiencing a reduction in activities such as transportation and  
216 construction that are sources of urban air pollution (Mohan & Kandya, 2007; Dhammapala, 2019);  
217 while industrial emitters such as those associated with steel production and power generation in  
218 the east continued (Reddy & Ruj, 2003; Singh et al., 2018) A similar pattern was seen along the  
219 Himalaya with decreases in the west and increases in the east.

220         This pattern is also consistent with anecdotal observations indicating that, for the first time  
221 in recent history, the visibility of Himalayan peaks from India's National Capital region (Chamas,  
222 2020; Ellis-Petersen et al., 2020). A persistent atmospheric anomaly characterized by cyclonic  
223 (counter-clockwise) air flow throughout the lower troposphere during April 2020 contributed to  
224 the dipolar pattern seen in both the IGP and Himalaya. These results confirm the importance of  
225 characterizing the spatial distribution of emissions across the IGP as well as the background  
226 atmospheric circulation when assessing the impact of pollution on the Himalaya. They also

227 provide an important test case that can be used to assess the ability of chemical transport models  
 228 to capture regional patterns in air quality in the presence of large-scale changes in emissions  
 229 (Moorthy et al., 2013; Sharma et al., 2017).

## 230 **Acknowledgments**

231 G.W.K.M. was supported by the Natural Sciences and Engineering Research Council of  
 232 Canada.

233 All satellite data was accessed through the NASA Goddard Earth Sciences (GES) Data and  
 234 Information Services Center (disc.gsfc.nasa.gov). Surface NO<sub>2</sub> data is available from the OpenAQ  
 235 Platform (openaq.org) and the Indian Open Government Data Platform (data.in.gov). Data on  
 236 pm<sub>2.5</sub> concentrations is available through the U.S. Environmental Protection Agency  
 237 (airnow.gov/international/us-embassies-and-consulates). ERA5 data is available through the  
 238 Copernicus Climate Data Store (cds.climate.copernicus.eu).

239

240

## 240 **References**

241

242 Aplin, K. L., Scott, C. J., & Gray, S. L. (2016). Atmospheric changes from solar eclipses.

243 *Philosophical Transactions of the Royal Society A: Mathematical, Physical and*  
 244 *Engineering Sciences*, 374(2077), 20150217.

245 <https://royalsocietypublishing.org/doi/abs/10.1098/rsta.2015.0217>

246 Begum, B. A., Biswas, S. K., & Hopke, P. K. (2011). Key issues in controlling air pollutants in  
 247 Dhaka, Bangladesh. *Atmospheric environment*, 45(40), 7705-7713.

248 <http://www.sciencedirect.com/science/article/pii/S1352231010008848>

249 Boersma, K., Eskes, H., Dirksen, R., Veefkind, J., Stammes, P., Huijnen, V., et al. (2011). An  
 250 improved tropospheric NO<sub>2</sub> column retrieval algorithm for the Ozone Monitoring  
 251 Instrument. *Atmospheric Measurement Techniques*, 4(9), 1905-1928.

252 Bonasoni, P., Cristofanelli, P., Marinoni, A., Vuillermoz, E., & Adhikary, B. (2012).

253 Atmospheric pollution in the Hindu Kush–Himalaya region. *Mountain Research and*  
 254 *Development*, 32(4), 468-479.

255 Brasseur, G., & Granier, C. (1992). Mount Pinatubo aerosols, chlorofluorocarbons, and ozone  
 256 depletion. *Science*, 257(5074), 1239-1242.

257 Chamas, Z. (2020). Peaks of Himalayas visible from parts of India for first time in decades as  
 258 pollution drops amid lockdown. Retrieved from <https://www.abc.net.au/news/2020-04-09/himalayas-visible-india-pollution/12136856>

259

- 260 Dentener, F., Stevenson, D., Ellingsen, K. v., Van Noije, T., Schultz, M., Amann, M., et al.  
 261 (2006). The global atmospheric environment for the next generation. *Environmental*  
 262 *Science & Technology*, 40(11), 3586-3594.
- 263 Dhammapala, R. (2019). Analysis of fine particle pollution data measured at 29 US diplomatic  
 264 posts worldwide. *Atmospheric environment*, 213, 367-376.
- 265 Ellis-Petersen, H., Ratcliffe, R., Cowie, W., Daniels, J. P., & Kuo, L. (2020, April 11 2020). It's  
 266 positively alpine!': Disbelief in big cities as air pollution falls. *The Guardian*.
- 267 Fishman, J., Creilson, J. K., Wozniak, A. E., & Crutzen, P. J. (2005). Interannual variability of  
 268 stratospheric and tropospheric ozone determined from satellite measurements. *Journal of*  
 269 *Geophysical Research: Atmospheres*, 110(D20).  
 270 <https://agupubs.onlinelibrary.wiley.com/doi/abs/10.1029/2005JD005868>
- 271 Ghude, S. D., Kulkarni, P. S., Kulkarni, S. H., Fadnavis, S., & Van Der A, R. (2011). Temporal  
 272 variation of urban NO<sub>x</sub> concentration in India during the past decade as observed from  
 273 space. *International journal of remote sensing*, 32(3), 849-861.
- 274 Hersbach, H., Bell, B., Berrisford, P., Hirahara, S., Horányi, A., Muñoz-Sabater, J., et al. (2020).  
 275 The ERA5 global reanalysis. *Quarterly Journal of the Royal Meteorological Society*,  
 276 146(730), 1999-2049. <https://rmets.onlinelibrary.wiley.com/doi/abs/10.1002/qj.3803>
- 277 Hong, G., Yang, P., Minnis, P., Hu, Y. X., & North, G. (2008). Do contrails significantly reduce  
 278 daily temperature range? *Geophysical Research Letters*, 35(23).
- 279 Korrick, S. A., Neas, L. M., Dockery, D. W., Gold, D. R., Allen, G. A., Hill, L. B., et al. (1998).  
 280 Effects of ozone and other pollutants on the pulmonary function of adult hikers.  
 281 *Environmental health perspectives*, 106(2), 93-99.
- 282 Lau, W. K., & Kim, K. M. (2010). Fingerprinting the impacts of aerosols on long-term trends of  
 283 the Indian summer monsoon regional rainfall. *Geophysical Research Letters*, 37(16).
- 284 Lippmann, M. (1989). Health Effects of Ozone A Critical Review. *JAPCA*, 39(5), 672-695.  
 285 <https://doi.org/10.1080/08940630.1989.10466554>
- 286 Mohan, M., & Kandya, A. (2007). An analysis of the annual and seasonal trends of air quality  
 287 index of Delhi. *Environmental monitoring and assessment*, 131(1-3), 267-277.
- 288 Moore, G., & Semple, J. (2009). High concentration of surface ozone observed along the  
 289 Khumbu Valley Nepal April 2007. *Geophysical Research Letters*, 36(14).
- 290 Moorthy, K. K., Beegum, S. N., Srivastava, N., Satheesh, S. K., Chin, M., Blond, N., et al.  
 291 (2013). Performance evaluation of chemistry transport models over India. *Atmospheric*  
 292 *environment*, 71, 210-225.  
 293 <http://www.sciencedirect.com/science/article/pii/S1352231013000812>
- 294 Pandey, M. (1984). Prevalence of chronic bronchitis in a rural community of the Hill Region of  
 295 Nepal. *Thorax*, 39(5), 331-336.
- 296 Pawar, V. S., Domkaware, M., Pawar, S., Salvekar, P., & Pradeep Kumar, P. (2017). Inter annual  
 297 variability of tropospheric NO<sub>2</sub> and tropospheric ozone over Maharashtra (India): the  
 298 role of lightning. *Remote Sensing Letters*, 8(11), 1015-1024.
- 299 Ramanathan, V., Ramana, M. V., Roberts, G., Kim, D., Corrigan, C., Chung, C., & Winker, D.  
 300 (2007). Warming trends in Asia amplified by brown cloud solar absorption. *Nature*,  
 301 448(7153), 575-578. <https://doi.org/10.1038/nature06019>
- 302 Reddy, G., & Ruj, B. (2003). Ambient air quality status in Raniganj-Asansol area, India.  
 303 *Environmental monitoring and assessment*, 89(2), 153-163.
- 304 Saikawa, E., Panday, A., Kang, S., Gautam, R., Zusman, E., Cong, Z., et al. (2019). Air Pollution  
 305 in the Hindu Kush Himalaya. In P. Wester, A. Mishra, A. Mukherji, & A. B. Shrestha

- 306 (Eds.), *The Hindu Kush Himalaya Assessment: Mountains, Climate Change,*  
 307 *Sustainability and People* (pp. 339-387). Cham: Springer International Publishing.
- 308 Semple, J. L., Moore, G. K., Koutrakis, P., Wolfson, J. M., Cristofanelli, P., & Bonasoni, P.  
 309 (2016). High concentrations of ozone air pollution on Mount Everest: Health implications  
 310 for Sherpa communities and mountaineers. *High altitude medicine & biology*, 17(4), 365-  
 311 369.
- 312 Sharma, S., Sharma, P., & Khare, M. (2017). Photo-chemical transport modelling of tropospheric  
 313 ozone: A review. *Atmospheric environment*, 159, 34-54.  
 314 <http://www.sciencedirect.com/science/article/pii/S1352231017302170>
- 315 Singh, R. P., Kumar, S., & Singh, A. K. (2018). Elevated black carbon concentrations and  
 316 atmospheric pollution around Singrauli coal-fired thermal power plants (India) using  
 317 ground and satellite data. *International journal of environmental research and public*  
 318 *health*, 15(11), 2472.
- 319 Torres, O., Tanskanen, A., Veihelmann, B., Ahn, C., Braak, R., Bhartia, P. K., et al. (2007).  
 320 Aerosols and surface UV products from Ozone Monitoring Instrument observations: An  
 321 overview. *Journal of Geophysical Research: Atmospheres*, 112(D24).  
 322 <https://agupubs.onlinelibrary.wiley.com/doi/abs/10.1029/2007JD008809>
- 323 Travis, D. J., Carleton, A. M., & Lauritsen, R. G. (2004). Regional variations in US diurnal  
 324 temperature range for the 11–14 September 2001 aircraft groundings: Evidence of jet  
 325 contrail influence on climate. *Journal of climate*, 17(5), 1123-1134.
- 326 Veefkind, J., Aben, I., McMullan, K., Förster, H., De Vries, J., Otter, G., et al. (2012).  
 327 TROPOMI on the ESA Sentinel-5 Precursor: A GMES mission for global observations of  
 328 the atmospheric composition for climate, air quality and ozone layer applications. *Remote*  
 329 *Sensing of Environment*, 120, 70-83.
- 330 WHO. (2006). *Air quality guidelines for particulate matter, ozone, nitrogen dioxide and sulfur*  
 331 *dioxide: global update 2005: summary of risk assessment*. Retrieved from  
 332

### 333 **Figure Captions**

334 Figure 1) Topography (m) and place names in the region of interest. The locations of New  
 335 Delhi ('+'), Ludhiana ('#'), Singrauli ('o'), Asansol ('x'), Lahore ('l'), Kathmandu ('k')  
 336 and Dhaka ('d') are indicated. Political boundaries are shown by the thin black curves  
 337 with the 3000m topographic height shown by the thick black curve.

338 Figure 2) Time series of surface NO<sub>2</sub> concentration (µg/m<sup>3</sup>) across the region of interest for the  
 339 period December 1 2019-May 1 2020. Results are shown for: a) Delhi; b) Ludhiana; c)  
 340 Singrauli and d) Asansol . The blue dashed lines represent the means over Feb 15-  
 341 March 15 and April 1-30. In a) the red curve is the climatological daily mean

342 concentration based on available data 2005-2019 with the red dashed/dotted curves  
343 representing one/two standard deviation above and below the climatological mean. A 31  
344 day moving window smoother has been applied to the climatological data.

345 Figure 3) Time series of surface  $\text{pm}_{2.5}$  ( $\mu\text{g}/\text{m}^3$ ) at selected sites in the region of interest for the  
346 period December 1 2019-April 24 2020. Results are shown for: a) Delhi; b) Lahore; c)  
347 Dhaka and d) Kathmandu .The blue dashed lines represent the mean over Feb 15-March  
348 15 and April 1-30. In a) the red curve is the climatological daily mean concentration  
349 based on available data 2016-2019 with the red dashed curves representing one standard  
350 deviation above and below the climatological mean. A 31 day moving window smoother  
351 has been applied to the climatological data. Also shown with the dashed blue line is the  
352 WHO standard for acceptable daily mean concentration ( $25 \text{ mg}/\text{m}^3$ ).

353 Figure 4) Column tropospheric  $\text{NO}_2$  density from the OMI ( $\text{m mol}/\text{m}^2$ ) across the region of  
354 interest. Results are shown for: a) April 1-30 climatology over 2005-2020 and b) April 1-  
355 30 2020. The locations of New Delhi ('+'), Ludhiana ('#'), Singrauli ('o'), Asansol ('x'),  
356 Lahore ('l'), Kathmandu ('k') and Dhaka ('d') are indicated. Political boundaries are  
357 shown by the thin black curves with the 3000m topographic height shown by the thick  
358 black curve.

359 Figure 5) Anomalous column tropospheric  $\text{NO}_2$  density from the OMI across the region of  
360 interest during April 2020. Results are shown for the: a) anomaly ( $\mu \text{ mol}/\text{m}^2$ ) b) the  
361 normalized anomaly (%). The locations of New Delhi ('+'), Ludhiana ('#'), Singrauli  
362 ('o'), Asansol ('x'), Lahore ('l'), Kathmandu ('k') and Dhaka ('d') are indicated.

363 Political boundaries are shown by the thin black curves with the 3000m topographic  
364 height shown by the thick black curve.

365 Figure 6) Column tropospheric NO<sub>2</sub> density ( $\mu\text{ mol/m}^2$ ) from the TROPOMI across the region  
366 of interest. Results are shown for: a) April 1-30 2019; b) April 1-30 2020 and c) the  
367 difference between April 1-30 2020 and 2019. The locations of New Delhi ('+'),  
368 Ludhiana ('#'), Singrauli ('o'), Asansol ('x'), Lahore ('l'), Kathmandu ('k') and Dhaka  
369 ('d') are indicated. Political boundaries are shown by the thin black curves with the  
370 3000m topographic height shown by the thick black curve.

371 Figure 7) The Aerosol Index from OMI across the region of interest. Results are shown for: a)  
372 April 1-30 climatology over 2005-2020; b) April 1-30 2020 and c) the normalized anomaly  
373 (%) for April 1-30 2020. The locations of New Delhi ('+'), Ludhiana ('#'), Singrauli ('o'),  
374 Asansol ('x'), Lahore ('l'), Kathmandu ('k') and Dhaka ('d') are indicated. Political  
375 boundaries are shown by the thin black curves with the 3000m topographic height shown  
376 by the thick black curve.

377 Figure 8) The tropospheric circulation across the region of interest during April 2020. The  
378 anomaly in the mass weighted wind (m/s) is shown. The locations of New Delhi ('+'),  
379 Ludhiana ('#'), Singrauli ('o'), Asansol ('x'), Lahore ('l'), Kathmandu ('k') and Dhaka ('d')  
380 are indicated. Political boundaries are shown by the thin black curves with the 3000m  
381 topographic height shown by the thick black curve.

382

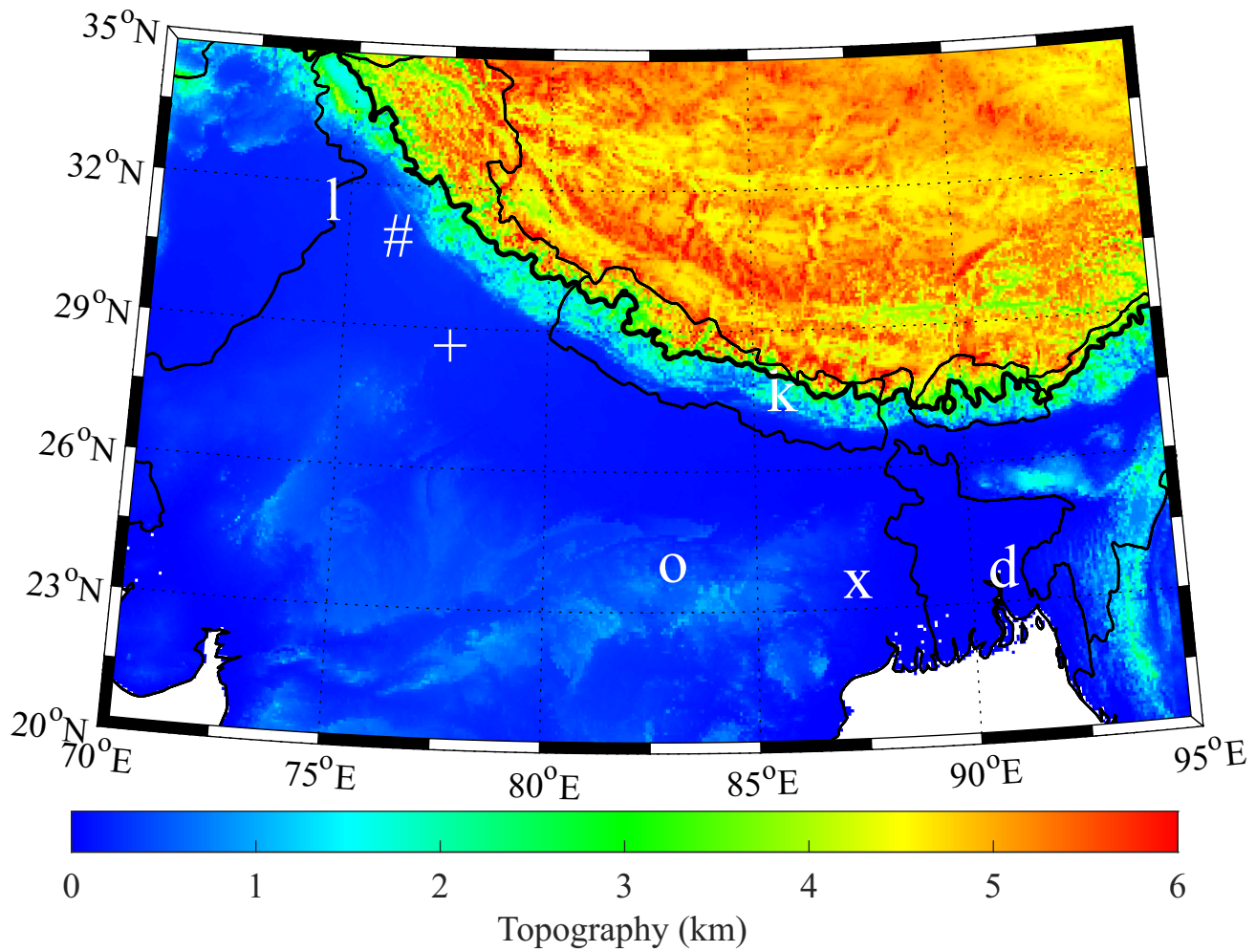


Figure 1) Topography (m) and place names in the region of interest. The locations of New Delhi ('+'), Ludhiana ('#'), Singrauli ('o'), Asansol ('x'), Lahore ('l'), Kathmandu ('k') and Dhaka ('d') are indicated. Political boundaries are shown by the thin black curves with the 3000m topographic height shown by the thick black curve.

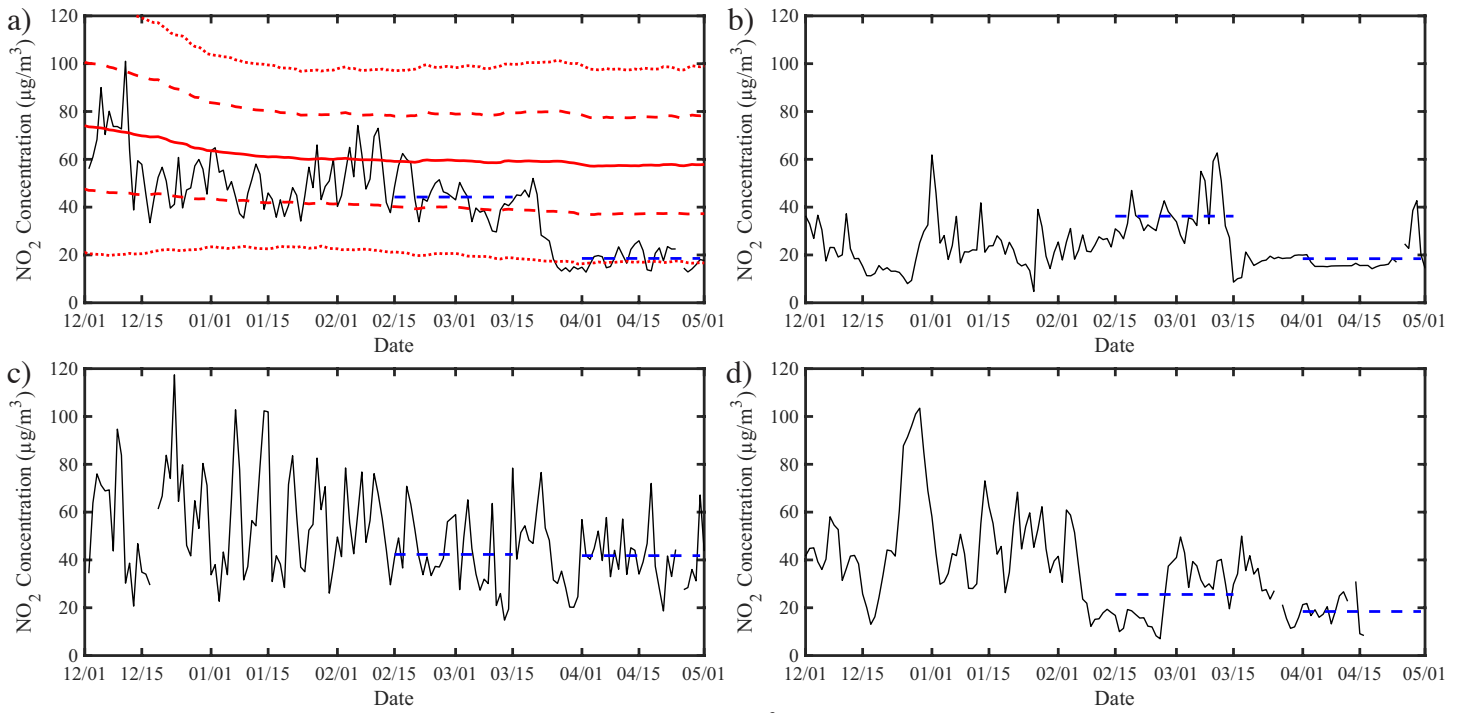


Figure 2) Time series of surface NO<sub>2</sub> concentration ( $\mu\text{g}/\text{m}^3$ ) across the region of interest for the period December 1 2019-May 1 2020. Results are shown for: a) Delhi; b) Ludhiana; c) Singrauli and d) Asansol. The blue dashed lines represent the means over Feb 15-March 15 and April 1-30. In a) the red curve is the climatological daily mean concentration based on available data 2005-2019 with the red dashed/dotted curves representing one/two standard deviation above and below the climatological mean. A 31 day moving window smoother has been applied to the climatological data.

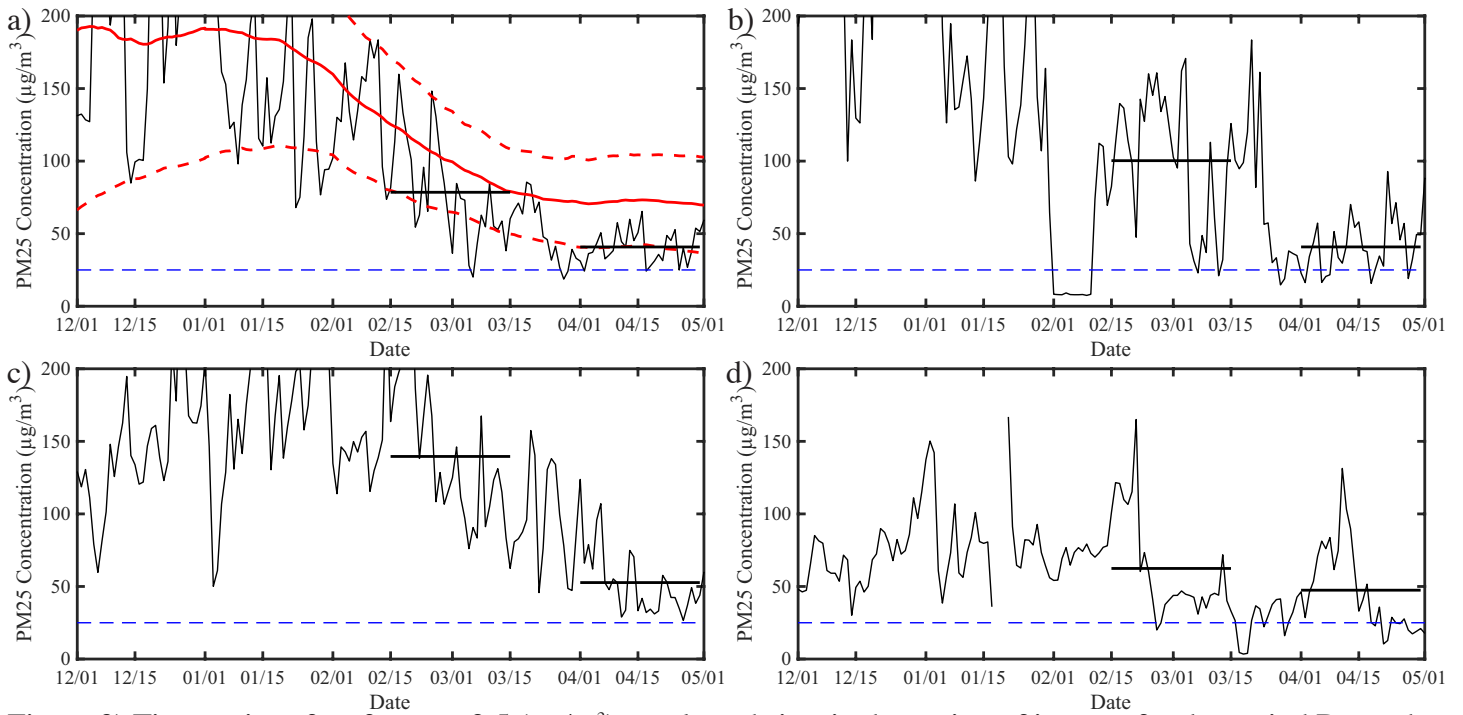


Figure 3) Time series of surface pm2.5 ( $\mu\text{g}/\text{m}^3$ ) at selected sites in the region of interest for the period December 1 2019-April 24 2020. Results are shown for: a) Delhi; b) Lahore; c) Dhaka and d) Kathmandu .The blue dashed lines represent the mean over Feb 15-March 15 and April 1-30. In a) the red curve is the climatological daily mean concentration based on available data 2016-2019 with the red dashed curves representing one standard deviation above and below the climatological mean. A 31 day moving window smoother has been applied to the climatological data. Also shown with the dashed blue line is the WHO standard for acceptable daily mean concentration ( $25 \text{ mg}/\text{m}^3$ ).

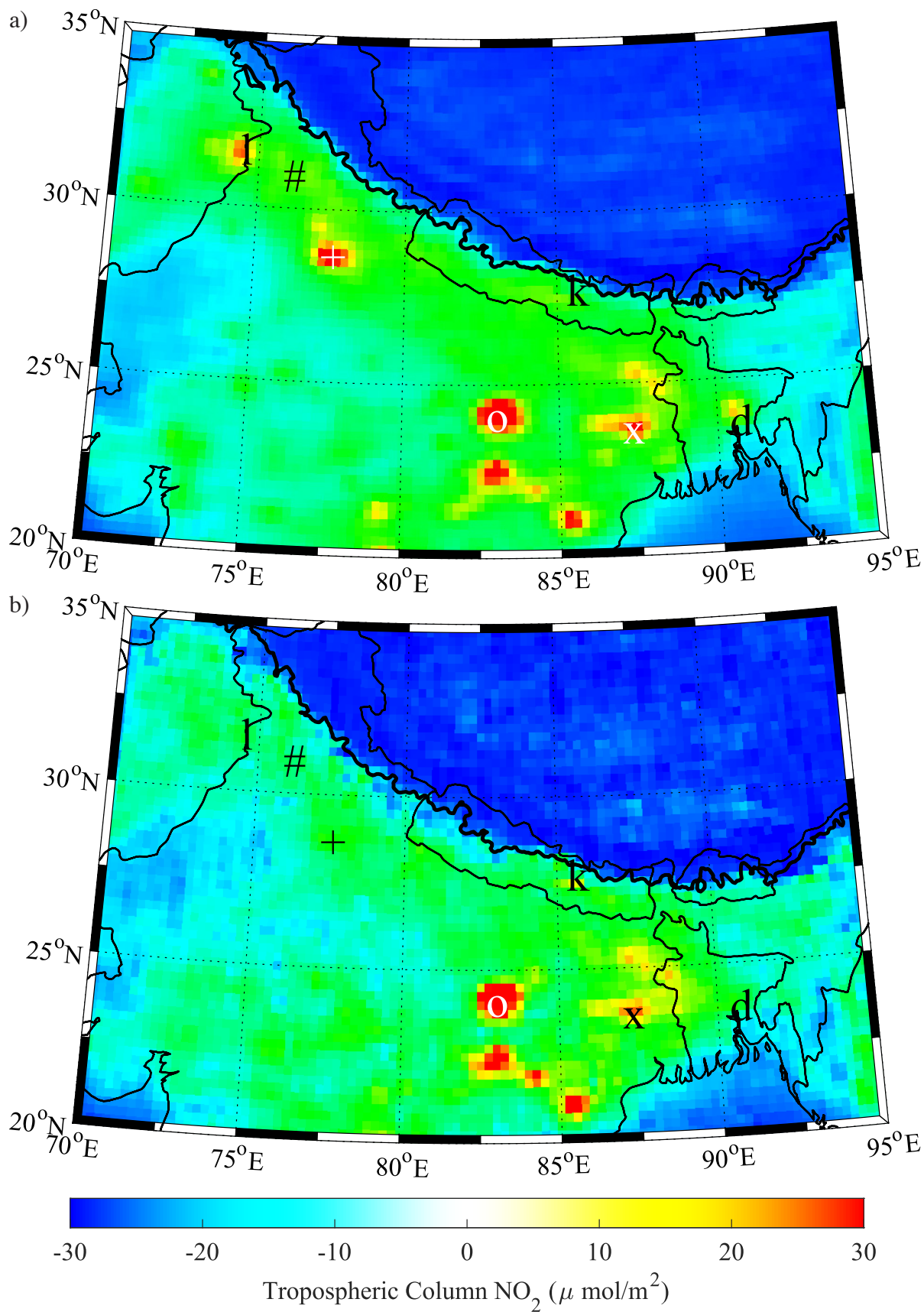


Figure 4) Column tropospheric NO<sub>2</sub> density from the OMI ( $\mu \text{ mol/m}^2$ ) across the region of interest. Results are shown for: a) April 1-30 climatology over 2005-2020 and b) April 1-30 2020. The locations of New Delhi ('+'), Ludhiana ('#'), Singrauli ('o'), Asansol ('x'), Lahore ('l'), Kathmandu ('k') and Dhaka ('d') are indicated. Political boundaries are shown by the thin black curves with the 3000m topographic height shown by the thick black curve.

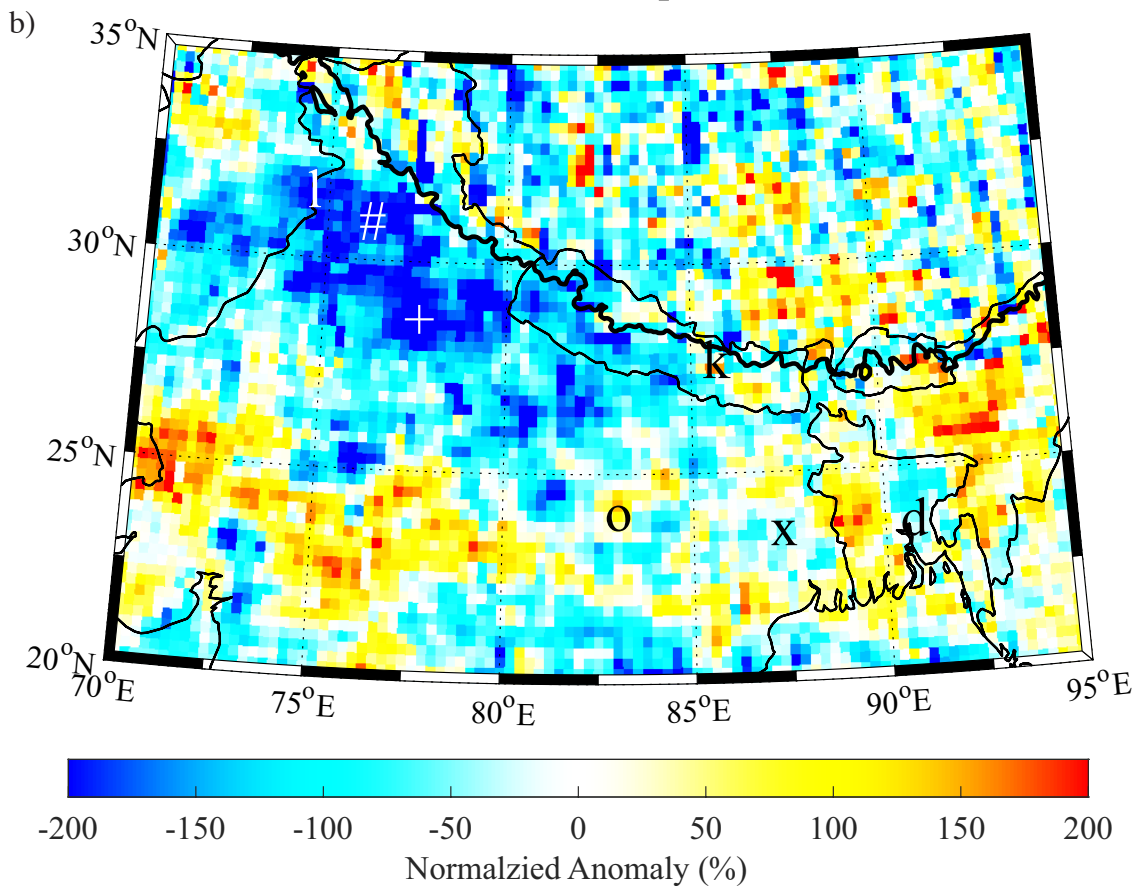
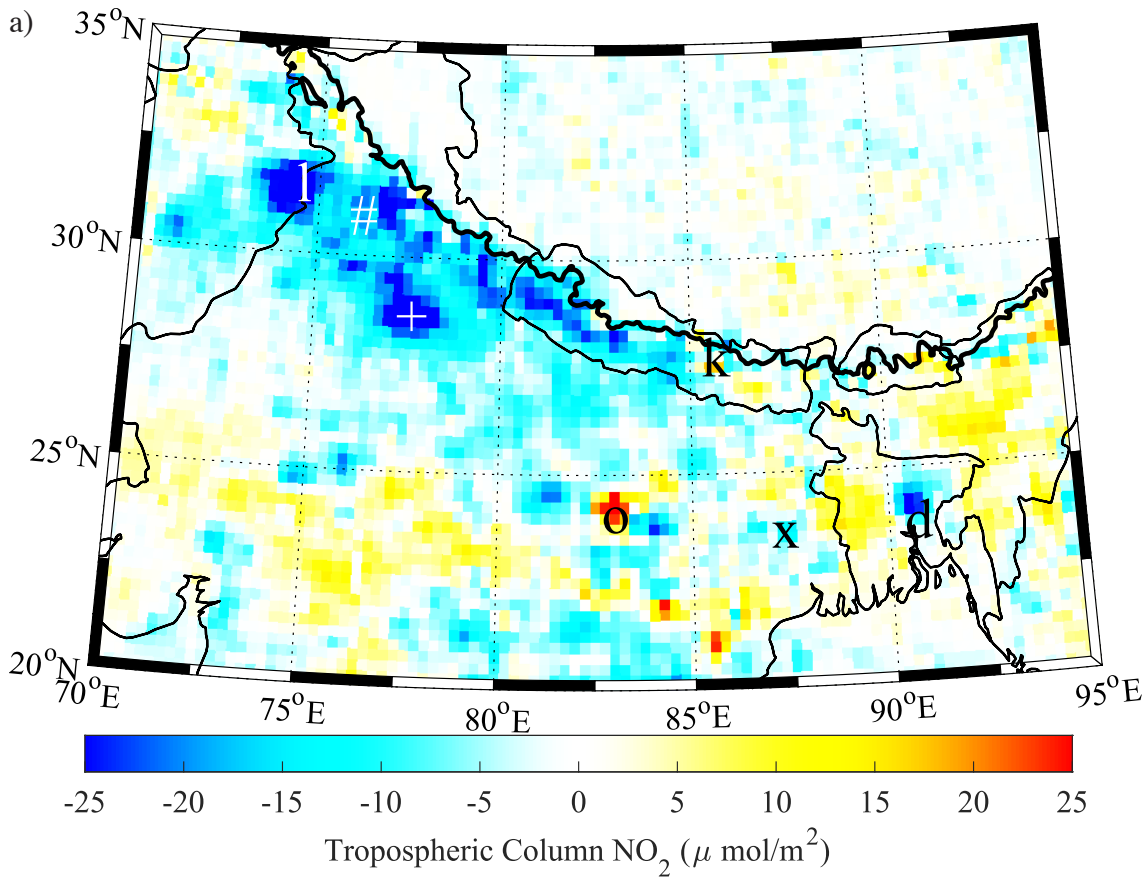


Figure 5) Anomalous column tropospheric NO<sub>2</sub> density from the OMI across the region of interest during April 2020. Results are shown for the: a) anomaly ( $\mu$  mol/m<sup>2</sup>) b) the normalized anomaly (%). The locations of New Delhi ('+'), Ludhiana ('#'), Singrauli ('o'), Asansol ('x'), Lahore ('l'), Kathmandu ('k') and Dhaka ('d') are indicated. Political boundaries are shown by the thin black curves with the 3000m topographic height shown by the thick black curve.

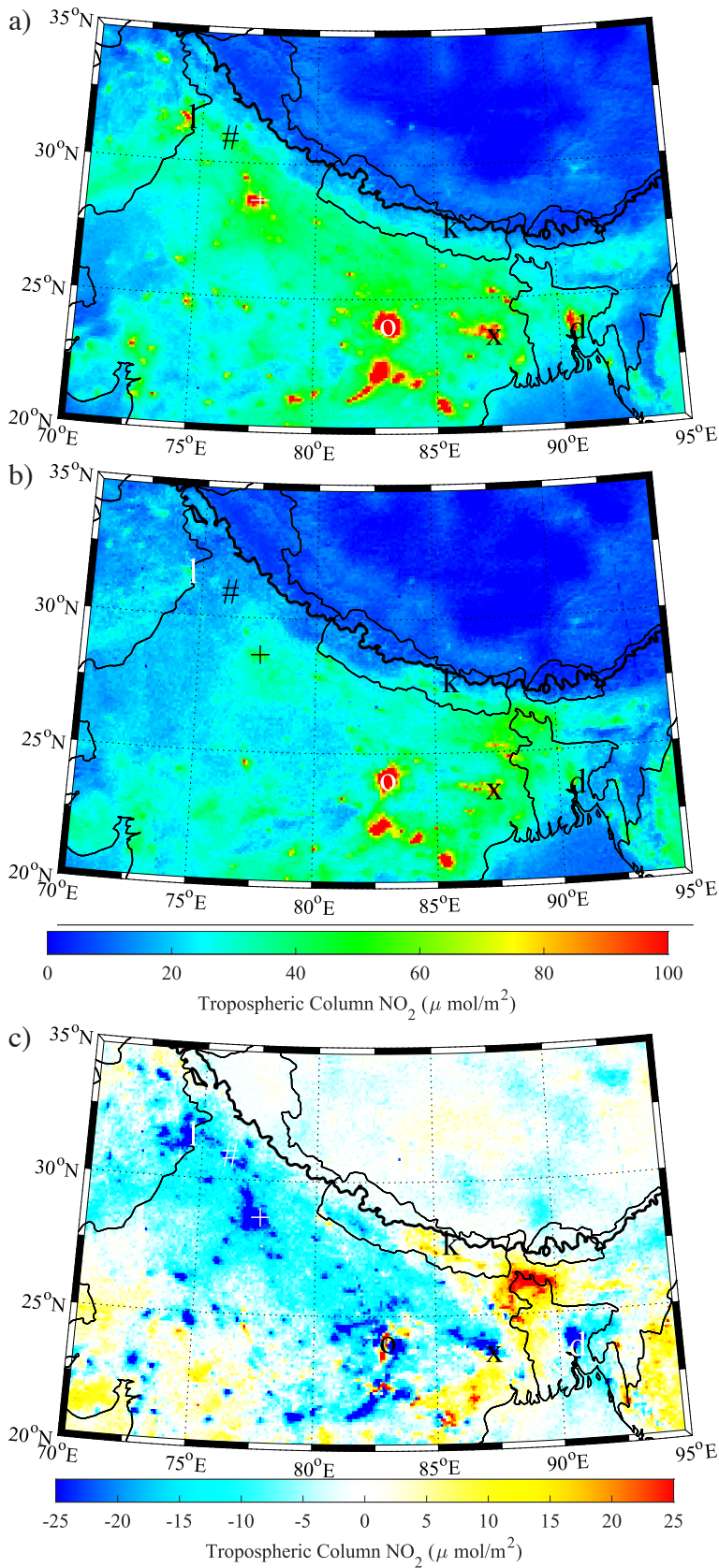


Figure 6) TROPOMI column tropospheric NO<sub>2</sub> density (μ mol/m<sup>2</sup>) for: a) April 1-30 2019; b) April 1-30 2020 and c) the difference between April 1-30 2020 and 2019. The locations of New Delhi ('+'), Ludhiana ('#'), Singrauli ('o'), Asansol ('x'), Lahore ('l'), Kathmandu ('k') and Dhaka ('d') are indicated. Political boundaries are shown by the thin black curves with the 3000m topographic height shown by the thick black curve.

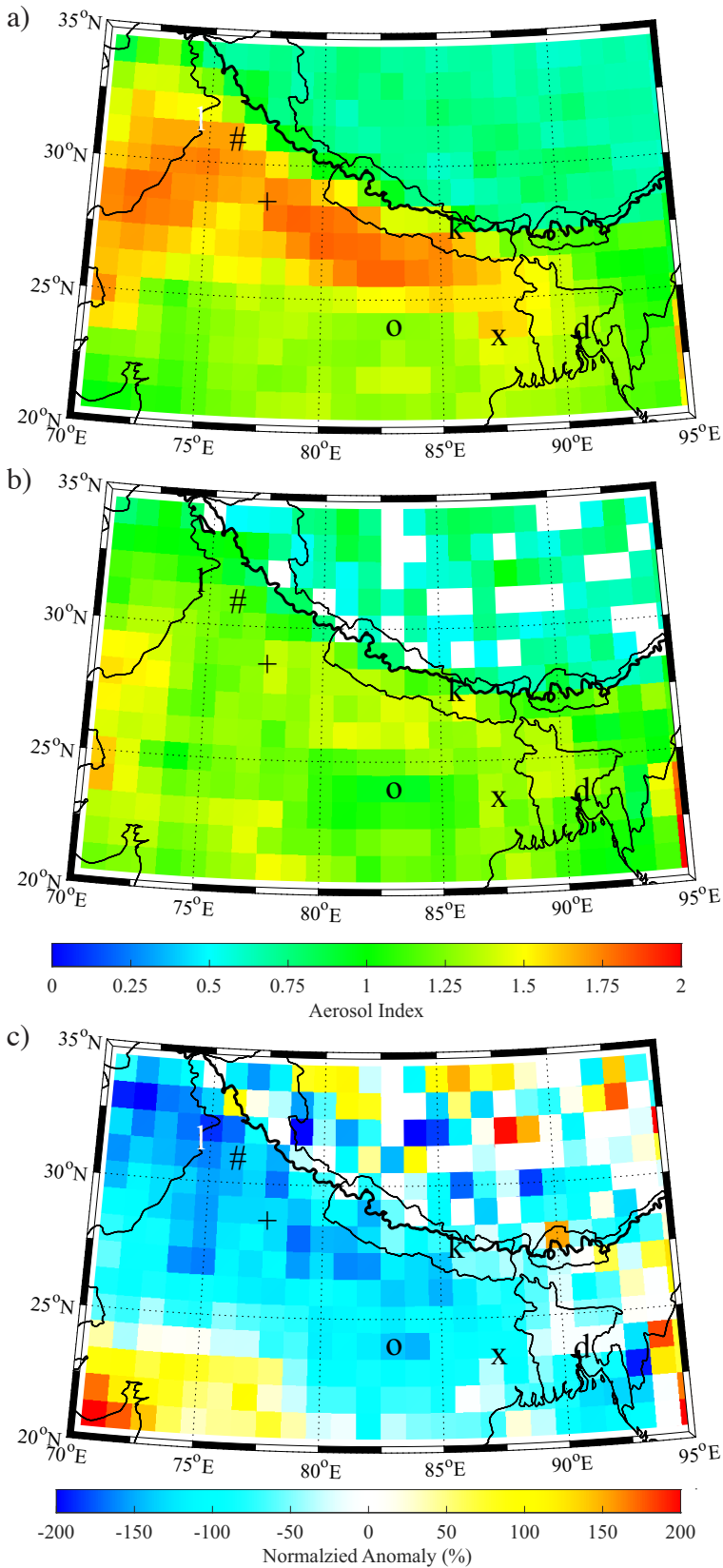


Figure 7) Column tropospheric NO<sub>2</sub> density ( $\mu\text{ mol/m}^2$ ) from the TROPOMI across the region of interest. Results are shown for: a) April 1-30 2019; b) April 1-30 2020 and c) the difference between April 1-30 2020 and 2019. The locations of New Delhi ('+'), Ludhiana ('#'), Singrauli ('o'), Asansol ('x'), Lahore ('l'), Kathmandu ('k') and Dhaka ('d') are indicated. Political boundaries are shown by the thin black curves with the 3000m topographic height shown by the thick black curve.

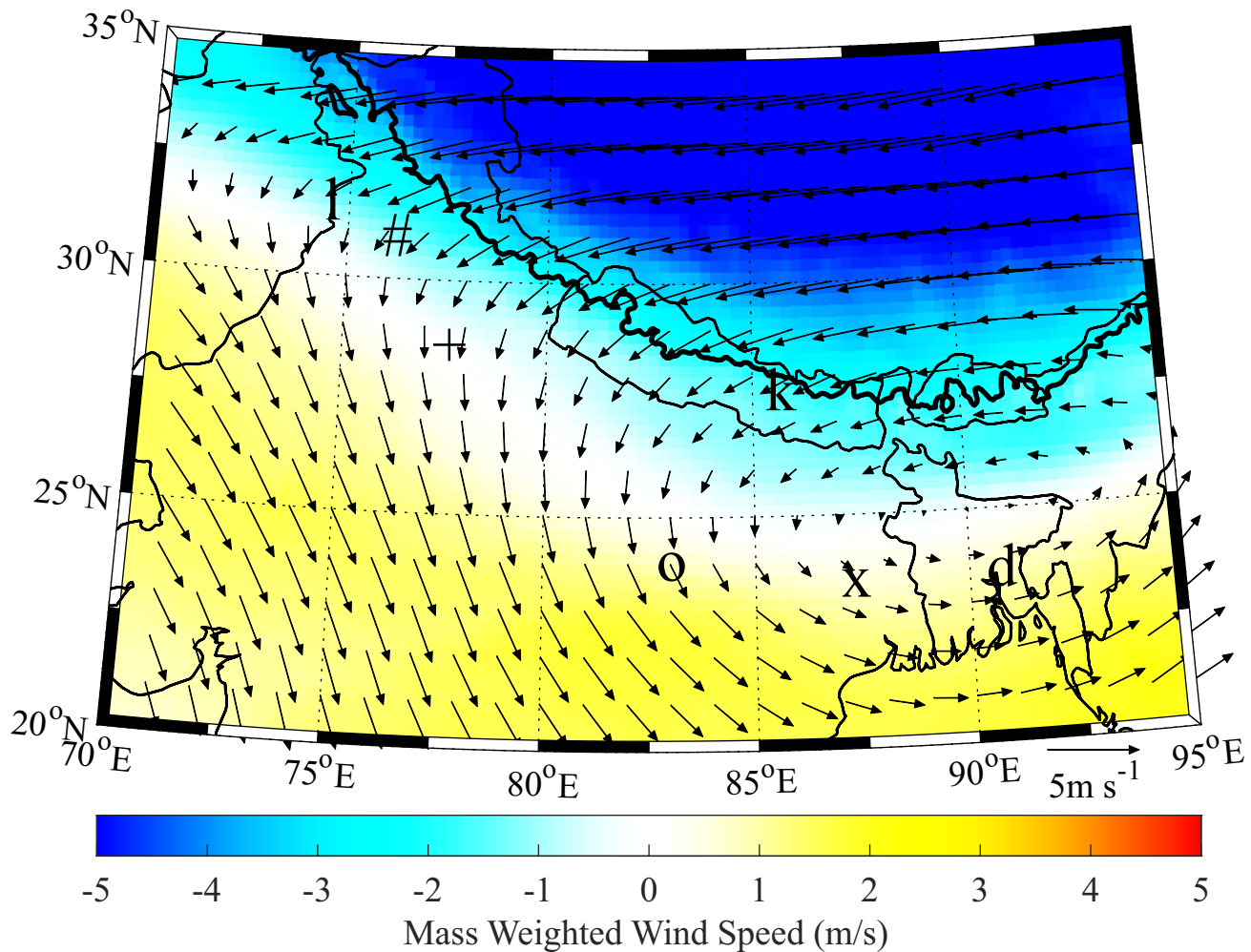


Figure 8) The tropospheric circulation across the region of interest during April 2020. The anomaly in the mass weighted wind (m/s) is shown. The locations of New Delhi ('+'), Ludhiana ('#'), Singrauli ('o'), Asansol ('x'), Lahore ('l'), Kathmandu ('k') and Dhaka ('d') are indicated. Political boundaries are shown by the thin black curves with the 3000m topographic height shown by the thick black curve.